


Cite this: *CrystEngComm*, 2022, 24, 8219

Four ternary silicides in the La–Ni–Si system: from polyanionic layers to frameworks†

Marcella Pani, ^{*ab} Alessia Provino,^{ab} Volodymyr Smetana, ^c Vitalii Shtender, ^e Cristina Bernini,^b Anja-Verena Mudring ^{*cd} and Pietro Manfrinetti ^{*ab}

The central part of the La–Ni–Si system has been investigated at 800 °C by means of single crystal X-ray diffraction, microscopy and analytical microprobe techniques. The result led to the identification of four new metal-rich silicides: LaNi₂Si (*R* $\bar{3}$ *m*, *a* = 4.0263(3) Å, *c* = 15.066(2) Å, *Z* = 3), La₂Ni₃Si₂ (*P*2₁/*c*, *a* = 6.8789(7) Å, *b* = 6.2167(3) Å, *c* = 12.214(1) Å, β = 90.92(1), *Z* = 4), La₃Ni₃Si₂ (*Pnma*, *a* = 7.501(2) Å, *b* = 14.316(4) Å, *c* = 6.149(2) Å, *Z* = 4), La₆Ni₇Si₄ (*Pbcm*, *a* = 6.066(1) Å, *b* = 7.488(1) Å, *c* = 29.682(5) Å, *Z* = 4). LaNi₂Si belongs to the SrCu₂Ga structure type, which is not represented among silicides, while La₂Ni₃Si₂ crystallizes in its own structure type. Both compounds feature layered polyanionic motifs consisting of Ni and Si, which are separated by La. Instead, La₆Ni₇Si₄ and La₃Ni₃Si₂ are characterized by polyanionic networks. The former compound belongs to the Pr₆Ni₇Si₄ structure type, with only two other representatives (Ce and Nd); the latter has been observed only with Rh and Ir. The two structures reveal close structural relationships having multiple identical slabs. Tight-binding electronic structure calculations by linear muffin-tin-orbital methods were performed for LaNi₂Si, La₂Ni₃Si₂ and La₃Ni₃Si₂ to gain insights into their structure–bonding relationships. Their band structures suggest a metallic character for all compounds. The overall crystal orbital Hamilton populations are dominated by polar Ni–Si bonds, though homoatomic Ni–Ni and La–Ni(Si) bond contributions are not negligible. The variety of bonding patterns may serve as a logical explanation for the number of discovered compounds in this system as well as for the diversity of the observed structures.

Received 23rd July 2022,
Accepted 19th September 2022

DOI: 10.1039/d2ce01007k

rsc.li/crystengcomm

Introduction

Among intermetallic compounds, silicides form an extensive class, comprehensively studied in both fundamental and applied research.¹ In particular, ternary compounds formed by Si in combination with a rare earth element and a transition metal are interesting due to the richness of their compositions and structural arrangements,² as well as their magnetic behavior,^{3,4} magnetocaloric,^{5,6} possible hydrogen sorption^{7,8}

and superconducting properties.^{9,10} Furthermore, silicides possess high corrosion resistance and thermal stability, being usually refractory materials with high melting points. For these reasons they show potential in technological applications; noteworthy, silicon is a very abundant element in nature and does not present any particular supply problem.

Therefore, further exploration of silicide systems has substantial benefits not only for further increasing structural diversity stimulating also the developments of related fields but also for design possibilities for direct applications. Particularly, silicides allow easy detection of new phases that can then be translated for other metalloids or transition metals (particularly 4d or 5d) to address manipulation towards desired physical properties.

Despite a large number of literature data on both the formation and crystal structure of *R*–Ni–Si system compounds,² knowledge about them is still far to be complete. Up to now, the phase equilibria in the *R*–Ni–Si system are still not established and the real number of existing compounds remains unknown owing to the richness and complexity of phase relationships. Although these systems have been intensively explored in the past,² new compounds can still be discovered. Particularly, the systems

^a DCCI, Department of Chemistry and Industrial Chemistry, University of Genova, Via Dodecaneso 31, I-16146, Genova, Italy. E-mail: marcella.pani@unige.it, pietro.manfrinetti@unige.it

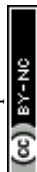
^b CNR-SPIN, Corso Perrone 24, I-16152, Genova, Italy

^c Department of Materials and Environmental Chemistry, Stockholm University, 10691 Stockholm, Sweden. E-mail: anja-verena.mudring@mmk.su.se

^d Department of Chemistry and iNANO, 253 Aarhus University, 8000 Aarhus C, Denmark

^e Department of Chemistry – Ångström Laboratory, Uppsala University, Box 538, 75121 Uppsala, Sweden

† Electronic supplementary information (ESI) available: Additional crystallographic information, Fig. S1 to S5; Tables S1–S3. CCDC 2149842–2149845 contain the supplementary crystallographic data for this paper. For crystallographic data in CIF or other electronic format see DOI: <https://doi.org/10.1039/d2ce01007k>



with Ce (ref. 11) and Gd (ref. 12) have been revisited recently resulting in more than 20 ternary compounds each. Most of them are located at the central part of the compositional triangle, and some of them have broad homogeneity regions hindering the establishment of the equilibria in the system.

The La–Ni–Si system has been explored in the past resulting in at least 19 reported structure representatives (LaNiSi: LaPtSi type, *tI12-I4₁md*; LaNiSi₂: CeNiSi₂ type, *oS16-Cmcm*; LaNi₂Si₂: CeAl₂Ga₂ type, *tI10-I4/mmm*; La(Ni_{0.5}Si_{1.5}): AlB₂ type, *hP3-P6/mmm*; La₂NiSi: Ce₅Ni₂Si₃ type, *hP40-P6₃/m*; LaNi₄Si: YNi₄Si type, *oS12-Cmmm*; La₃Ni₄Si₄: U₃Ni₄Si₄ type, *oI22-Immm*; La₃Ni₃Si₇: Ce₃Ni₂Si₈ type, *oS26-Cmmm*; La₇Ni₂Si₅: Ce₇Ni₂Si₅ type, *oP56-Pnma*; La₃NiSi₃: Ba₃Al₂Ge₂ type, *oI14-Immm*; LaNi₉Si₂: CeNi₈(Ni_{0.6}Si_{0.4})Si₂ type, *tI48-I4₁/amd*; LaNi_{13-x}Si_x: NaZn₁₃ type, *cF112-Fm3c*; LaNi₉Si₄: LaFe₉Si₄ type, *tI56-I4/mcm*; LaNi₆Si₆: CeNi₆Si₆ type, *tP52-P4/nbm*; La₆Ni_{1.5}Si₃: Nd₆Ni_{1.66}Si₃ type, *hP26-P6₃/m*; La₅Ni_{1.8}Si₃: its own type, *hP44-P6₃/m*; La₁₅Ni_{6.6}Si₁₀: its own type, *hP68-P6₃/m*; La₂₁Ni₁₀Si₁₅: its own type, *hP98-P6₃/m*; La₁₄Ni₆Si₁₁: Pr₁₄Ni₆Si₁₁ type, *mS124-C2/m*),^{2,7,13–15} one of which, La₂₁Ni_{10.49}Si₁₅,¹⁶ has never been observed in any of the related systems with other *R*. From the structural point of view, the system shows a tendency towards the homological series, e.g. the compound series La_{(n+1)(n+2)}Ni_{n(n-1)+2}Si_{n(n+1)} (*n* = 2–5) based on AlB₂ type building blocks.¹⁶ LaNiSi (ref. 9) and La₃Ni₄Si₄ (ref. 17) revealed superconducting behavior, while LaNi_{5-x}Si_x have been studied for hydrogen sorption¹⁸ and battery applications.¹⁹ The isothermal section of the La–Ni–Si system at 400 °C has been suggested.¹⁴ Nevertheless, due both to the high formation temperatures of rare earth-transition metal-silicides and the difficulty to obtain appreciable diffusion rates of the elements in the solid state, we decided to study the system at 800 °C. Indeed, our current investigation immediately revealed that certain parts of the phase space remained unexplored or differ significantly at higher temperatures, particularly the area La–LaNiSi–Ni, thus suggesting possible space for expansion.

In this work, we report the synthesis and structural characterization of four new La–Ni silicides: LaNi₂Si, La₂Ni₃Si₂, La₃Ni₃Si₂ and La₆Ni₇Si₄. LaNi₂Si belongs to the SrCu₂Ga structure type,²⁰ which is not represented among silicides, while La₂Ni₃Si₂ crystallizes in its own structure type. Both compounds exhibit a layered type of structure. La₆Ni₇Si₄ and La₃Ni₃Si₂ instead are characterized by polyanionic networks. The former one belongs to the Pr₆Ni₇Si₄ structure type with Ce and Nd homologues reported as other representatives,²¹ while the latter has been observed only with Rh and Ir.² The investigation has been performed employing X-ray diffraction, microscopy analysis and first-principle calculations. Detailed analysis of structural motifs of the new compounds in comparison to known ones is presented as well.

Experimental

Synthesis

Different samples were synthesized in the ternary system La–Ni–Si, exploring the composition ranges 24–46 at% La, 37–50

at% Ni and 15–32 at% Si. The alloys were prepared starting from pure elements: La pieces (99.9 wt%), Ni slugs (99.99 wt%) and Si grains (99.999 wt%). Samples with a total mass of about 2–3 g each were arc melted in a high-purity argon atmosphere, after the fusion of a Ti–Zr alloy as a getter. The buttons were remelted at least twice after turning them upside-down to ensure good homogenization. After melting, the as-cast samples were placed in Ta containers, closed in evacuated fused silica tubes and annealed at 750–800 °C for 6–12 days. At the end of the heat treatment, they were cooled down to room temperature by switching off the furnace.

Microscopy analysis

Both light optical microscopy (LOM) and scanning electron microscopy (SEM) equipped with an energy dispersive X-ray (EDX) microprobe (Leica Cambridge S360, Oxford X-Max20 spectrometer, with Aztec software) were employed to check the homogeneity of the samples and the phase composition. In the case of SEM/EDX, after standard micrographic preparation, the specimens were graphitized and analyzed at a working distance of 25 mm, with an accelerating voltage of 20 kV. For all samples, in addition to a global compositional analysis, at least three different points or areas for each phase present were analyzed. Moreover, a ternary compound with known and fixed stoichiometry, such as LaNi₂Si₂, was used as a reference to check for the accuracy of the atomic percentage of La, Ni and Si elements; in this way, the measurements were estimated to be accurate within ±0.5 atom %. The nominal compositions of the synthesized samples, annealing conditions and results of EDX analyses are presented in Table 1. Fig. S1† shows the microstructural appearance of samples no. 3, 4, 5, 6, 8 and 9, selected as the best representatives.

X-ray analysis

X-ray diffraction, both on powders and single crystals, was employed for structural characterization. Powder patterns were collected using a Panalytical powder diffractometer (Bragg–Brentano geometry, Ni-filtered CuKα or Fe-filtered CoKα radiation) in the 10–120° 2θ range, with 0.02° 2θ step and counting times of 15–20 s per step. For precise determination of lattice parameters, silicon powder was added as an internal standard to the sample powders. Single-crystal X-ray diffraction (XRD) measurements were performed at room temperature on a Bruker D8 Venture diffractometer operating at 50 kV and 1.4 mA equipped with a Photon 3 CMOS detector, a flat graphite monochromator, and a Mo Kα IμS 3.0 microfocus source (λ = 0.71073 Å). The raw frame data were collected using the Bruker APEX3 software package (Bruker AXS, 2015), while the frames were integrated with the Bruker SAINT program using a narrow-frame algorithm for the integration of the data and were corrected for absorption effects using the multiscan method (SADABS).²² Initial models of the crystal structures were first obtained with the program SHELXT-2014 (ref. 23) and refined using the



Table 1 Prepared samples and results of the elemental and phase analyses

Sample no.	Nominal composition (at%) La : Ni : Si	Annealing conditions	Composition detected by EDX (at%) La : Ni : Si		Phases detected by PXRD
			Global	Observed phases	
1	45.6 : 39.4 : 15	800 °C – 9 days	45.4 : 39.3 : 15.3	A 37.2 : 37.6 : 25.2 matrix B 51 : 18.1 : 30.9	A La ₃ Ni ₃ Si ₂ main phase B La ₅ Ni _{1.75} Si ₃
2	37.5 : 37.5 : 25.0	800 °C – 9 days	37.3 : 37.5 : 25.2	Monophasic	La ₃ Ni ₃ Si ₂
3	34 : 44 : 22	800 °C – 12 days	34.8 : 42.1 : 23.1	A 35.8 : 39.5 : 24.7 matrix B 25.8 : 48.4 : 25.8 globular crystals C 34.0 : 43.3 : 22.7 traces D 41.4 : 56.0 : 2.6 traces	A La ₆ Ni ₇ Si ₄ main phase B LaNi ₂ Si C ≈ La ₃ Ni ₄ Si ₂ unknown D La ₂ (Ni ₃ Si) ₃
4	33.3 : 43.4 : 23.3	800 °C – 9 days	33.3 : 43.1 : 23.6	A 35.3 : 41.5 : 23.2 matrix B 28.3 : 43.5 : 28.2 large crystals C 25 : 49.9 : 25.1 traces, dark crystals D 50.2 : 49.8 traces, white phase	A La ₆ Ni ₇ Si ₄ main phase B La ₂ Ni ₃ Si ₂ C LaNi ₂ Si D ≈ LaNi
5	32 : 46 : 22	750 °C – 8 days	32.6 : 44.6 : 22.8	A 36 : 40 : 24 matrix B 25.8 : 48.4 : 25.8 dark crystals C 34.0 : 43.3 : 22.7 traces D 41.4 : 56.0 : 2.6 traces	A La ₆ Ni ₇ Si ₄ main phase B LaNi ₂ Si C ≈ La ₃ Ni ₄ Si ₂ unknown D La ₂ (Ni ₃ Si) ₃
6	28.4 : 43.4 : 28.2	800 °C – 9 days	28.5 : 43.1 : 28.4	Monophasic	A La ₂ Ni ₃ Si ₂ main phase B impurity traces
7	25 : 50 : 25	800 °C – 6 days	25.9 : 48.5 : 25.6	A 26.1 : 48.5 : 25.4 matrix B 26.3 : 41.9 : 31.8 traces C 20.7 : 38.8 : 40.5 traces	A LaNi ₂ Si main phase B ≈ La ₂ Ni ₄ Si ₃ unknown C LaNi ₂ Si ₂ traces
8	25 : 45 : 30	800 °C – 9 days	25 : 45 : 30	A 25.1 : 49.1 : 25.8 majority phase B 24.5 : 43 : 32.5 secondary phase C 20 : 39.6 : 40.4 traces	A LaNi ₂ Si main phase B ≈ La ₂ Ni ₄ Si ₃ unknown C LaNi ₂ Si ₂ traces
9	24.6 : 43.4 : 32	800 °C – 9 days	24.4 : 43.5 : 32.1	A 25.7 : 43.9 : 30.4 matrix B 20.4 : 39.9 : 39.7 acicular crystals	A ≈ La ₂ Ni ₄ Si ₃ unknown, main phase B LaNi ₂ Si ₂

program SHELXL-2014 (ref. 24) within the APEX3 software package. The atomic displacement parameters were refined anisotropically for all atoms. STRUCTURE TIDY²⁵ was used for the atomic coordinate standardization and Diamond (Crystal Impact GmbH, 2015) for the structural drawings. Single crystal data and relevant parameters of the intensity data collections and structure refinements are presented in Table S1.† Representative XRD powder patterns (samples no. 2, 5, 6, 7, 9) are presented in the ESI,† Fig. S2 to S4.

DTA analysis

During the investigation, selected samples were subjected to differential thermal analysis (DTA) to explore phase transformations as a function of temperature up to ~1400 °C, by using a NETZSCH 404S DTA thermal analyzer. A specimen of the alloy (~0.5–0.8 g), prepared and annealed as described above, was placed inside an alumina crucible and transferred to the DTA apparatus. The heating and cooling cycles were run at rates of 20 and 10 °C min⁻¹, respectively, with a temperature measurement accuracy of about 5 °C.

Electronic structure calculations

Tight binding electronic structure calculations for all compounds were performed according to the linear muffin-tin-orbital (LMTO) method in the atomic sphere approximation (ASA).^{26,27} The radii of the Wigner–Seitz spheres were assigned automatically so that the overlapping potentials would be the best possible approximations to the

full potentials.²⁸ The radii for La, Ni and Si were determined to be in the ranges 1.87–2.19, 1.29–1.44 and 1.36–1.39 Å, respectively. Three empty spheres for LaNi₂Si and eleven for La₃Ni₃Si₂, respectively, were required for space filling in the ASA with 16% overlap restrictions between atom-centered spheres. Basis sets of La 6s, (6p), 5d, Ni 4s, 4p, 3d and Si 3s, 3p (downfolded orbitals in parentheses) were employed. For bonding analyses, the energy contributions of all filled electronic states for selected atom pairs were calculated as a function of energy by the COHP method (crystal orbital Hamilton population) and the integrated values up to the Fermi energy, –ICOHPs.²⁹ Total energy calculations and structure optimizations (unit cell volume and shape plus atomic coordinates) for LaNi₂Si in its own structure and a hypothetical CaNi₂Si structure type (Table S3†) have been performed using the VASP³⁰ following the procedure described elsewhere.³¹

Results and discussion

LaNi₂Si

The occurrence of a compound with the composition LaNi₂Si was detected in five different samples with nominal compositions ranging between 25 and 34 at% of La; none of these samples was found to be perfectly monophasic. Even when prepared on its precise composition, or on a composition very close to the nominal one (samples 7 and 8), traces of the 1:2:2 and of the not yet known ~2:4:3 secondary phases were obtained (Fig. S3†). The DTA analysis



performed on the $\text{La}_{25}\text{Ni}_{50}\text{Si}_{25}$ sample (no. 7) showed two thermal effects of comparable magnitude, at 1040 and 985 °C, respectively. In this regard, it should be noted that, in spite of the many samples analyzed by DTA, a clear and reliable interpretation of the data obtained has not been achieved so far. Indeed, every sample is generally characterized by a sequence of several thermal events, which follow one another in a cascade. Due to this, it is not possible at the moment to attribute the formation/decomposition of the phases reported in this work to any thermal effect. The DTA analysis of further samples subjected to various thermal treatments is currently underway. A single crystal, isolated from sample 3 (Table 1), indicated a small rhombohedral cell with the lattice parameters $a = 4.0263(3)$ Å and $c = 15.066(2)$ Å. This unit cell was subsequently confirmed by X-ray powder diffraction analysis of the same sample, as well as detected in other pertinent samples. Taking into account the elemental volumes and considering the formula LaNi_2Si as suggested by the SEM analyses, a volume contraction $\Delta V = 11\%$ was calculated for $Z = 3$, in agreement with the typical values observed for other lanthanide–nickel silicides. The structure solution was obtained in the centrosymmetric space group $R\bar{3}m$.

LaNi_2Si belongs to the SrCu_2Ga type²⁰ representing a rather simple layered structure, in which hexagonal planes of La and Ni/Si alternate along the [001] direction (Fig. 1). While the La planes are perfectly planar, Ni and Si build corrugated $^{2/3}[\text{Ni}_2\text{Si}]$ layers, where each Si atom is in the center of a fused nickel hexagon exhibiting chair conformation. Accordingly, within the Ni–Si framework, each Ni atom adopts an “umbrella geometry”, being linked to 3 Ni and 3 Si atoms, while each Si atom is coordinated to 6 Ni atoms (Fig. 1b and c) in a trigonal-antiprismatic environment. The antiprisms are strongly compressed in the z direction. The thickness of the $^{2/3}[\text{Ni}_2\text{Si}]$ layers is about 0.93 Å considering Δz between the two Ni atoms delimiting the layer. The shortest interatomic contacts are realized by Ni and, in particular, values of $d/\sum r < 1$ are observed within the Ni/Si layer for the Ni–Si bonds ($d/\sum r$ is defined as the ratio between the experimental distance and the sum of the proper CN12 elemental radii³²). Noteworthy, no Si–Si contacts occur within the layers, as well as no interlayer bond contacts have

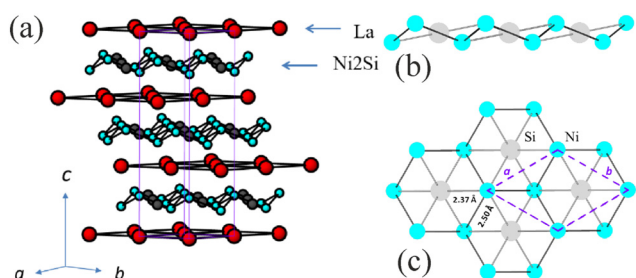


Fig. 1 The rhombohedral structure of LaNi_2Si viewed along the [110] direction, showing alternating layers of La and Ni_2Si stacked along c (a); the $^{2/3}[\text{Ni}_2\text{Si}]$ layer in LaNi_2Si , viewed along the [110] direction (b) and the [001] direction (c).

been observed. The shortest distances between adjacent Ni/Si layers ($d_{\text{Ni-Si}} = 4.56$ Å) are significantly larger than those within the layers ($d_{\text{Ni-Si}} = 2.37$ Å, $d_{\text{Ni-Ni}} = 2.50$ Å), emphasizing the two-dimensional character of the structure.

Besides LaNi_2Si , the SrCu_2Ga structure type is represented amongst transition metals only by BaCu_2Ga .²⁰ However, about 400 ternary intermetallic compounds formed by a lanthanide or an alkaline earth metal are known to crystallize with this composition (1:2:1, Parthé code 7533) being distributed among more than 10 different structure types (Table S2†).² In addition to the YPd_2Sn type (MnCu_2Al Heusler phase), which includes nearly 200 examples, and the YPd_2Si type (Fe_3C derivative) with nearly 60 representatives, the third most abundant family is the GdPt_2Sn (or ZrPt_2Al) type. In Pearson's Crystal Database (PCD),² the GdPt_2Sn compound is assigned to the LiCu_2Sn prototype that is correct up to the point where the formal cations exchange the $2a$ and $2c$ sites. Yet another alternative with the exchange of the Wyckoff positions is the Li_2CuAs type. CaNi_2Si is an ordered ternary derivative of the ReB_3 type,³³ referred to as a new type in PCD but is very closely related to the GdPt_2Sn type. Its hexagonal structure (Fig. 2) is characterized by the same “ Ni_2Si ” layers found in LaNi_2Si , though a certain shift in the ab plane is observed. Since these two structure types are very closely related, we decided to inspect them more thoroughly.

Despite the larger size of Ca, the normalized volume of CaNi_2Si per formula unit ($V_{\text{f.u.}} = \frac{V_{\text{cell}}}{Z}$) is noticeably lower compared to that of LaNi_2Si : 68.62 vs. 70.49 Å³. This in part can find a justification taking into account the substantial difference between the compressibility values of the two elements, $\chi_{\text{Ca}} = 64.51 \times 10^{-7}$ and $\chi_{\text{La}} = 40.37 \times 10^{-7} \text{ cm}^2 \text{ kg}^{-1}$,³⁴ respectively. Similarly, the normalized axial ratio $(c/a)_{\text{norm}}$

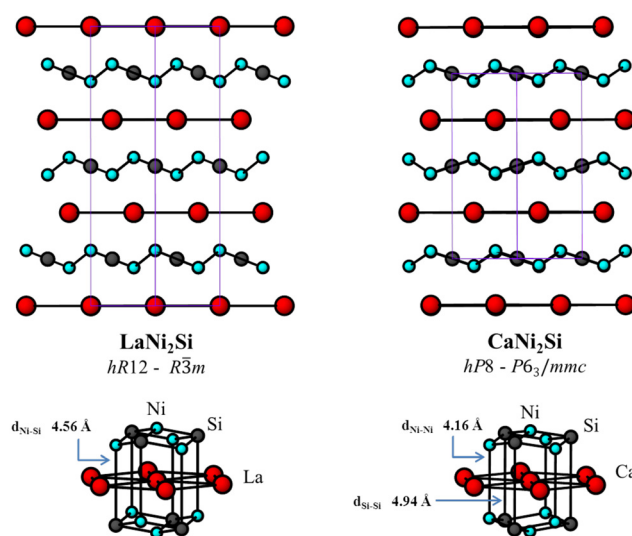


Fig. 2 Comparison between the crystal structures of LaNi_2Si and CaNi_2Si (viewed along the [110] direction) (top) and the coordination polyhedra around La and Ca (bottom).



and the height of the Ni/Si layer are slightly lower in CaNi_2Si (1.240 and 0.78 Å) than in LaNi_2Si (1.247 and 0.93 Å) resulting from the lower degree of corrugation of the Ni/Si layer in the Ca compound leading to higher compression along [001]. The intralayer Ni/Si contacts ($d_{\text{Ni-Si}} = 2.34$ Å and $d_{\text{Ni-Ni}} = 2.44$ Å) are shorter than those realized in LaNi_2Si (2.37 Å and 2.50 Å, respectively): a result related to the nature of Ca which is a better electron donor to the $^{2-}_{\infty}[\text{Ni}_2\text{Si}]$ polyanions.

An analysis of the total energies calculated for the optimized LaNi_2Si and CaNi_2Si in both structure types reveals notable energetic preferences for each cation in its experimentally observed structure type. Furthermore, we observed a negligible unit cell volume optimization for the same cation in different packing options. For instance, LaNi_2Si in the SrCu_2Ga structure shows 99 meV f.u.⁻¹ preference over the CaNi_2Si structure and 0.42 Å³ smaller unit cell. In contrast, CaNi_2Si in its own structure shows 101 meV f.u.⁻¹ preference over the SrCu_2Ga type packing and just 0.13 Å³ reduced volume. This suggests the indirect influence of the cation on volume optimization through reorganization/corrugation of the polyanionic framework. The calculations also highlight that none of the above structure types for each cation can be converted to another under applied external pressure.

$\text{La}_2\text{Ni}_3\text{Si}_2$

The SEM analysis performed on sample no. 4 ($\text{La}_{33.3}\text{Ni}_{43.4}\text{Si}_{23.3}$, see Table 1 and Fig. S1†) clearly revealed the polyphasic nature of the latter. Besides the main phase with composition $\sim\text{La}_{35}\text{Ni}_{42}\text{Si}_{23}$ (later identified as the $\text{La}_6\text{Ni}_7\text{Si}_4$ compound), and two compounds present in traces (LaNi_2Si and LaNi), a few well-grown grains were identified with the composition $\text{La}_{28.3}\text{Ni}_{43.5}\text{Si}_{28.2}$, which corresponds quite well to the fixed stoichiometry $\text{La}_2\text{Ni}_3\text{Si}_2$. A new sample, prepared with the nominal composition 2:3:2 (sample no. 6, Fig. S3†), was found to be nearly homogeneous. None of the known structures around the same compositional range (Parthé code: 7140) was compatible with the powder diffraction data. Data from a suitable crystal, isolated from the latter sample, led to a primitive monoclinic cell with lattice parameters $a \cong 6.8$ Å, $b \cong 6.2$ Å, $c \cong 12.2$ Å, and $\beta \cong 91^\circ$ bearing no similarity to any known phase reported in the literature, thus confirming a new structure type. The observed systematic absences pointed to the space group $P2_1/c$. The structure solution proceeded smoothly *via* direct methods, and the first seven peaks of the Fourier map were assigned to 2 La, 3 Ni and 2 Si all being fully occupied.

The crystal structure adopted by $\text{La}_2\text{Ni}_3\text{Si}_2$ is unique and is not directly related to other compounds of the 2:3:2 family. It exhibits clear layered motifs in which Ni and Si build wide puckered layers, extended parallel to the (100) planes and separated by La atoms (Fig. 3). The coordination polyhedra are rather irregular (Fig. S5†). La1 and La2 are characterized by high coordination numbers, CN19 and CN17, respectively, as expected for the elements with large

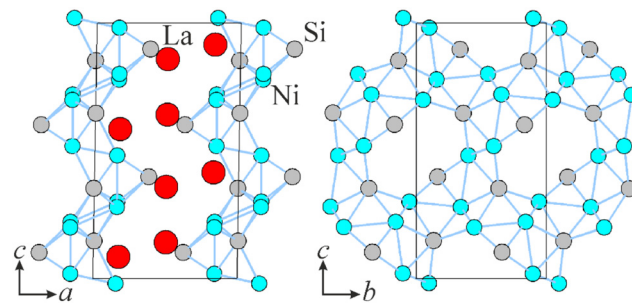


Fig. 3 (left) The monoclinic structure of $\text{La}_2\text{Ni}_3\text{Si}_2$ viewed along [010]; the interatomic bonds within the Ni-Si network are highlighted. (right) Projection of the single Ni-Si layer along [100].

size. Si1 is surrounded by 6 La and 6 Ni atoms, adopting a highly distorted icosahedral coordination while Si2 is nine-coordinated (6La + 3Ni) adopting a monocapped square antiprism. All Ni positions exhibit similarities in their coordination environments, which can be described as distorted trigonal prismatic with capped faces. All of them are equatorially tricapped, while Ni2 is additionally monocapped axially. It is also worth noting that in all cases the Ni coordination sphere contains a La_4 tetrahedron.

The complex interconnection of the Ni and Si atoms leads to highly corrugated layers. As a general observation, the atoms are arranged to maximize the number of Ni-Si contacts, adopting a coordination that resembles the “umbrella conformation” already observed in LaNi_2Si . The Ni-Si distances, being the shortest ones within the layer, are expected to give a major contribution to the stabilization of the entire polyanionic system. Notably, no Si-Si bonds are observed.

$\text{La}_3\text{Ni}_3\text{Si}_2$ and $\text{La}_6\text{Ni}_7\text{Si}_4$

Compounds with the nominal compositions of $\text{La}_3\text{Ni}_3\text{Si}_2$ and $\text{La}_6\text{Ni}_7\text{Si}_4$ were uncovered during systematic search of the possible isostructural compounds within $R\text{-T-Si}$ systems. While $\text{La}_3\text{Ni}_3\text{Si}_2$ resulted in a perfectly homogeneous sample, $\text{La}_6\text{Ni}_7\text{Si}_4$ was always observed in polyphasic samples (see Table 1 and Fig. S1†). Shiny crystals were easily observed in multiphase alloys. Both structures were established by single crystal X-ray diffraction. Later, PXRD analysis confirmed their occurrence in multiple samples in the investigated area (Table 1). Refinement details for both compounds as well as crystallographic details are presented in Table S1.†

$\text{La}_3\text{Ni}_3\text{Si}_2$ and $\text{La}_6\text{Ni}_7\text{Si}_4$ are strongly related, both compositionally and structurally (Fig. 4). Both of them crystallize in the orthorhombic system with the space groups $Pnma$ (*oP32*) and $Pbcm$ (*oP68*), respectively, and show complex polyanionic nets. $\text{La}_3\text{Ni}_3\text{Si}_2$ belongs to the $\text{Ce}_3\text{Rh}_3\text{Si}_2$ structure type,³⁵ while $\text{La}_6\text{Ni}_7\text{Si}_4$ to $\text{Pr}_6\text{Ni}_7\text{Si}_4$,²¹ both being quite underrepresented.

The crystal structure of $\text{La}_3\text{Ni}_3\text{Si}_2$ consists of a polyanionic Ni/Si network and zigzag chains of the La atoms along the *b* axis. For ease of describing, the polyanionic net can be split into separate alternating slabs (Fig. 4a). In this description,



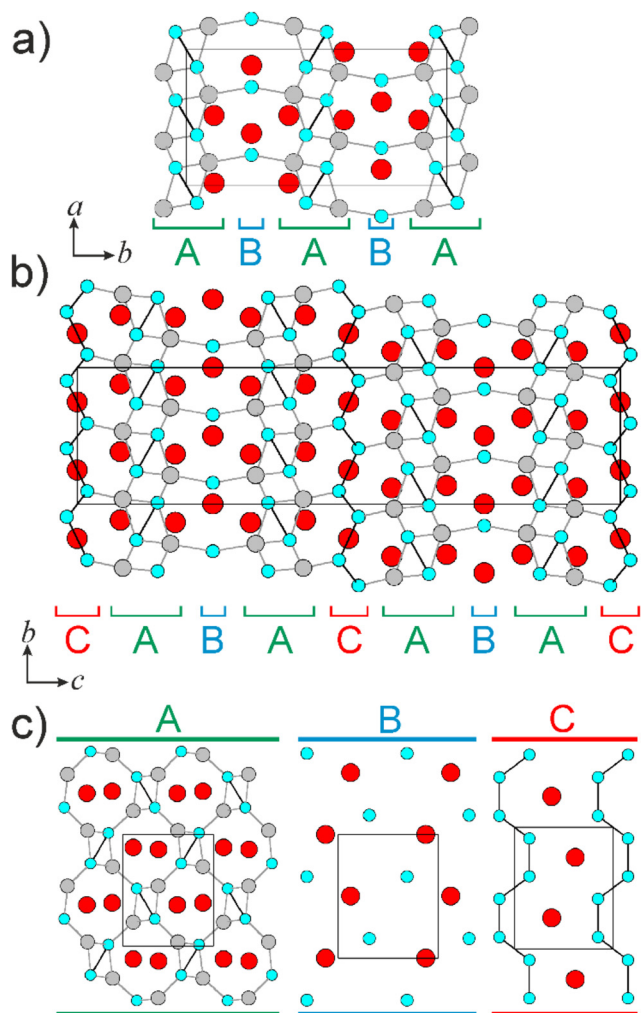


Fig. 4 Projection of the crystal structure of $\text{La}_3\text{Ni}_3\text{Si}_2$ on the ab plane (a), $\text{La}_6\text{Ni}_7\text{Si}_4$ on the bc plane (b) and projections of the constituent slabs identical for both structures (c). Each slab is color-coded A – green, B – blue and C – red. La atoms are red, Ni – blue, Si – gray.

we focus mainly on the polyanionic Ni/Si motifs. One of them, slab A ($\text{La}_2\text{Ni}_2\text{Si}_2$, Fig. 4c), represents a rhombi-octagonal tiling similar to that observed in the series of ternary trielides/tetralides with late transition metals – $\sim\text{A}_{0.5}\text{T}_2\text{X}_2$ (A = alkali metal, T = Pd, Pt, Au; X = Ga, In, Si, Ge),^{36–40} though is highly corrugated. A similar tiling is also present in $\text{La}_2\text{Ni}_3\text{Si}_2$, though the rhombi have common edges and the ratio of the octagons is lower. Slab B (LaNi) is represented solely by a distorted quadrangular net of the isolated Ni atoms serving as a bridge between two A slabs. The cations are regularly distributed along the b axis in a sinusoidal pattern.

The $\text{Pr}_6\text{Ni}_7\text{Si}_4$ structure type has been represented as an intergrowth of the ThSi_2 (ref. 41) and $\text{Y}_3\text{Rh}_2\text{Si}_2$ (ref. 42) structures with equally complex arrangements. However, similarly to $\text{La}_3\text{Ni}_3\text{Si}_2$, the crystal structure of $\text{La}_6\text{Ni}_7\text{Si}_4$ is more easily understood as an intergrowth of three different slabs (Fig. 4b). The slabs A (with nominal composition $\text{La}_2\text{Ni}_2\text{Si}_2$) and B (LaNi) are identical to those observed in $\text{La}_3\text{Ni}_3\text{Si}_2$. The A:B:C slab ratio in $\text{La}_6\text{Ni}_7\text{Si}_4$ is consequently 2:1:1. The cations form sinusoidal chains extending through all slabs

along the c axis and resemble, to some extent, the chains forming the layers in the crystal structure of the black phosphorus.⁴³ The connectivity between all the slabs in both compounds is established solely *via* heteroatomic Ni–Si bonding, however, these contacts are quite long and represent the upper edge of the Ni–Si bonding spectrum in the compounds – 2.665(1) and 2.649(2) Å, respectively. The same is valid for the interslab connectivity around C in $\text{La}_6\text{Ni}_7\text{Si}_4$, though the contacts are slightly shorter ($d_{\text{Ni–Si}} = 2.462(2)$ Å). The connectivity in the B slab is preferentially heteroatomic, though Ni–Ni bonding is not excluded. The Ni–Si contacts are considerably shorter – 2.307–2.376(2) Å. The Ni–Ni contacts are also quite short ($d_{\text{Ni–Ni}} = 2.565$ – $2.591(1)$ Å), slightly exceeding the sum of the covalent radii.⁴⁴ No Si–Si contacts have been observed in any of the structures.

Following the tendency observed in LaNi_2Si and $\text{La}_2\text{Ni}_3\text{Si}_2$, the coordination polyhedra are rather irregular. La coordination numbers range between 17 and 20. The Si positions are surrounded by seven La and four Ni atoms representing an overlap of a (capped) trigonal prism and a tetrahedron, respectively. The smallest Ni atoms are always 9- or 10-coordinated and their coordination sphere is a strongly distorted square antiprism (Fig. S5†).

Electronic structure and chemical bonding

The electronic densities-of-state (DOS) of the investigated compounds are shown in Fig. 5 and exhibit plenty of similar features. Broad s, p bands can be observed up to ~ 10 eV below the Fermi level (E_F), while large mostly Ni 3d bands are located 1–4 eV below E_F . Fermi levels for all compounds intersect pretty sizable DOS regions, suggesting metallic characteristics. The total density at the Fermi level is usually dominated by Ni 3d and La 5d states, while contributions from Si are significantly smaller. Above the Fermi level La 5d states start to dominate suggesting that La is mostly in the +III oxidation state in line with the element electronegativity differences,⁴⁵ therefore, serving to a large extent as an electron donor. Ni and Si states overlap practically in the

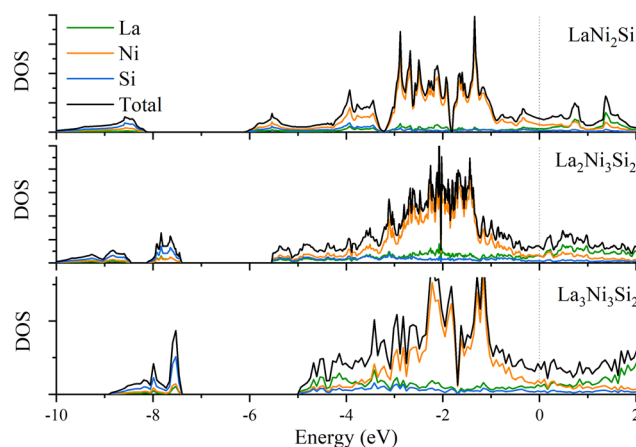


Fig. 5 Total and projected densities of states of LaNi_2Si , $\text{La}_2\text{Ni}_3\text{Si}_2$ and $\text{La}_3\text{Ni}_3\text{Si}_2$.



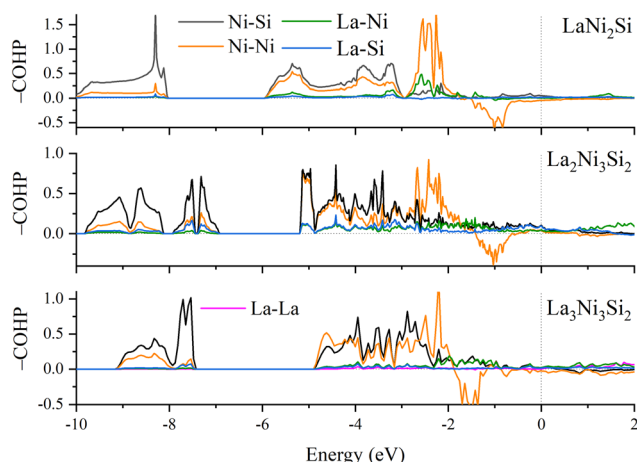


Fig. 6 $-COHP$ curves of $LaNi_2Si$, $La_2Ni_3Si_2$ and $La_3Ni_3Si_2$.

entire range both below and above the Fermi level in agreement with the strong covalent bonding observed between these elements in all structures.

COHP analysis shows that the Ni–Ni interactions are mostly of bonding nature becoming antibonding around 2 eV below the Fermi level and remaining negligibly antibonding at and above the E_F (Fig. 6). Overall these interactions are highly populated, that is rather typical for filled d^{10} – d^{10} interactions.^{31,46–48} Ni–Si contacts are strongly bonding at lower energies getting optimized at the Fermi level. Similar are the La–Ni and La–Si interactions, though their populations are significantly lower. It is worth noting that despite being a formal electron donor La participates actively in the covalent bonding interactions and their bond contributions are quite sizable (Table 2).

Of special interest is the bonding situation in $La_2Ni_3Si_2$ and $La_3Ni_3Si_2$. In both these structures particularly short (~ 2.3 Å) Ni–Si contacts could be observed being close to the sum of the covalent radii of these elements.⁴⁴ The shortest contacts are extremely highly populated with the $-ICOHP$ values of up to 2.9 eV per bond confirming strong bonding

character. It is worth noting that such bond contraction has particularly been observed in other representatives of the $Ce_3-Rh_3Si_2$ structure type³⁵ pointing to the high stability of the observed polyanionic layered structures in the silicides.⁴⁹ Similar bond contraction is also known in the series of active metal–gold trielides,^{50,51} explained by local coordination around the bond. Indeed, the Si positions in the crystal structure of $La_2Ni_3Si_2$ have a highly irregular coordination environment, with the limited amount of the Ni near neighbors (up to six) and the La atoms being practically beyond the first coordination sphere. The same is observed in both $La_3Ni_3Si_2$ and $La_6Ni_7Si_4$, with strictly four Ni near neighbors around the Si positions.

Both $La_3Ni_3Si_2$ and $La_6Ni_7Si_4$ exhibit quite short La–La contacts, 3.5040(9) Å and 3.4458(9) Å. Though La atoms participate in covalent bonding interactions, the $-ICOHP$ value of 0.04 eV per bond suggests rather weak direct La–La interactions. La is the most electropositive in the compound with a quite high electronegativity difference with both Ni and Si and must bear a certain positive charge. Taking into account the ionic component, the short La–La contacts surprisingly are not too resembling the connectivity between the active metals in the polyanionic Au/Ga tunnels.^{36,52}

Conclusions

We have presented the synthesis and the crystal structures of four new ternary compounds in the central part of the La–Ni–Si system exhibiting various polyanionic motifs. The atomic packing in $LaNi_2Si$ and $La_2Ni_3Si_2$ is of 2D polyanionic nature with either single or double Ni/Si corrugated layers. The latter are separated by either single flat La sheets or thicker double corrugated zigzag-shaped slabs, respectively. $La_3Ni_3Si_2$ and $La_6Ni_7Si_4$ form polyanionic frameworks closely related to each other with encapsulated cationic motifs. Two out of four newly discovered silicides, $LaNi_2Si$ and $La_3Ni_3Si_2$, showed close vicinity with the gallides, while the other two either belong to its own structure type ($La_2Ni_3Si_2$) or to a heavily

Table 2 Bond length ranges and average $-ICOHP$ values in $LaNi_2Si$, $La_2Ni_3Si_2$ and $La_3Ni_3Si_2$

Bond type	Lengths (Å)	$-ICOHP$ (eV per avg. bond)	<i>n</i> /cell	$-ICOHP$ (eV per cell)	Contribution (%)
$LaNi_2Si$					
Ni–Si	2.371	2.09	14	29.26	62.5
Ni–Ni	2.505	1.39	7	9.73	20.8
La–Ni	2.978–3.096	0.26	22	5.76	12.3
La–Si	3.422	0.13	16	2.08	4.4
$La_2Ni_3Si_2$					
Ni–Si	2.297–2.461	2.47	44	108.78	61.3
Ni–Ni	2.478–2.520	1.21	14	16.94	9.6
La–Ni	2.926–3.584	0.40	56	22.4	12.6
La–Si	3.118–3.782	0.46	64	29.2	16.5
$La_3Ni_3Si_2$					
Ni–Si	2.308–2.665	1.66	31	51.46	65.2
Ni–Ni	2.575	1.04	4	4.16	5.3
La–Ni	2.767–3.189	0.27	56	15.32	19.5
La–Si	3.119–3.631	0.14	56	7.76	9.8
La–La	3.504	0.04	4	0.16	0.2



underrepresented structure type ($\text{La}_6\text{Ni}_7\text{Si}_4$) with just a few other homologous silicides. To the best of our knowledge, those related systems have never been explored in detail, allowing broad exchange possibilities of practically all elements in the formula using the La–Ni–Si system as a starting point.

The total Ni–Si bond lengths observed are very close to the sum of the respective covalent radii confirming strong interactions. More detailed analyses of the electronic structures of selected compounds show that although all of them are metallic, the overall bond populations are strongly dominated by polar Ni–Si bonds. The homoatomic Ni–Ni contacts being comparatively strong are rarely observed and, therefore, contribute less to the total bonding schemes. Notably, the major involvement of La in covalent bonding interactions is observed in all compounds, though short La–La contacts in $\text{La}_3\text{Ni}_3\text{Si}_2$ together with low $-\text{ICOHP}$ values suggest large ionic components typically observed for all active metals in similar compounds. Despite the multiphasic nature of these samples, attempts to prepare single-phase materials of these compounds, to be measured, are underway.

Conflicts of interest

The authors declare no competing interest.

Acknowledgements

This research was supported, in part, by Energimyndigheten (grant no. P48699-1).

References

- 1 K. S. Kumar, Intermetallics: Silicides, in *Encyclopedia of Materials: Metals and Alloys*, ed. F. G. Caballero, Elsevier, Oxford, 2001, pp. 335–338.
- 2 P. Villars and K. Cenzual, *Pearson's Crystal Data – Crystal Structure Database for Inorganic Compounds*, ASM International, Materials Park, Ohio, USA, release 2018/19.
- 3 B. Malaman, G. Venturini, G. Le Caër, L. Pontonnier, D. Fruchart, K. Tomala and J. P. Sanchez, Magnetic structures of PrFeSi_2 and NdFeSi_2 from neutron and Mossbauer studies, *Phys. Rev. B: Condens. Matter Mater. Phys.*, 1990, **41**(7), 4700–4712, DOI: [10.1103/PhysRevB.41.4700](#).
- 4 P. Stefański and A. Wrzeciono, Structural and magnetic properties of $\text{RFe}_{10}\text{Si}_2$ compounds, *J. Magn. Magn. Mater.*, 1989, **82**(1), 125–128, DOI: [10.1016/0304-8853\(89\)90072-3](#).
- 5 A. O. Pecharsky, K. A. Gschneidner and V. K. Pecharsky, The giant magnetocaloric effect of optimally prepared $\text{Gd}_5\text{Si}_2\text{Ge}_2$, *J. Appl. Phys.*, 2003, **93**(8), 4722–4728, DOI: [10.1063/1.1558210](#).
- 6 F. Wang, G.-J. Wang, F.-X. Hu, A. Kurbakov, B.-G. Shen and Z.-H. Cheng, Strong interplay between structure and magnetism in the giant magnetocaloric intermetallic compound $\text{LaFe}_{11.4}\text{Si}_{1.6}$: a neutron diffraction study, *J. Phys.: Condens. Matter*, 2003, **15**(30), 5269–5278, DOI: [10.1088/0953-8984/15/30/309](#).
- 7 A. V. Morozkin, S. N. Klyamkin, V. N. Verbetsky, S. N. Lushnikov, V. K. Portnoy, E. A. Movlaev, A. P. Chernavskii and A. V. Tarasov, Hydrogen sorption in homologous lanthanum and cerium nickel silicides, *J. Alloys Compd.*, 2000, **309**(1), 197–200, DOI: [10.1016/S0925-8388\(00\)00981-6](#).
- 8 M. Pasturel, J. L. Bobet, O. Isnard and B. Chevalier, Unusual increase of the Kondo effect by hydrogenation: case of the ternary silicide CeNiSi , *J. Alloys Compd.*, 2004, **384**(1), 39–43, DOI: [10.1016/j.jallcom.2004.03.126](#).
- 9 W. H. Lee, F. A. Yang, C. R. Shih and H. D. Yang, Crystal structure and superconductivity in the Ni-based ternary compound LaNiSi , *Phys. Rev. B: Condens. Matter Mater. Phys.*, 1994, **50**(9), 6523–6525, DOI: [10.1103/PhysRevB.50.6523](#).
- 10 H. F. Braun, Superconductivity of rare earth-iron silicides, *Phys. Lett. A*, 1980, **75**(5), 386–388, DOI: [10.1016/0375-9601\(80\)90849-X](#).
- 11 A. V. Morozkin, A. V. Knotko, A. V. Garshev, V. O. Yapaskurt, R. Nirmala, S. Quezado and S. K. Malik, The Ce–Ni–Si system as a representative of the rare earth–Ni–Si family: Isothermal section and new rare-earth nickel silicides, *J. Solid State Chem.*, 2016, **243**, 290–303, DOI: [10.1016/j.jssc.2016.09.001](#).
- 12 A. V. Morozkin, A. V. Knotko, V. O. Yapaskurt, P. Manfrinetti, M. Pani, A. Provino, R. Nirmala, S. Quezado and S. K. Malik, The isothermal section of Gd–Ni–Si system at 1070 K, *J. Solid State Chem.*, 2016, **235**, 58–67, DOI: [10.1016/j.jssc.2015.12.019](#).
- 13 ICSD, FIZ-Karlsruhe, Karlsruhe, Germany, 2018.
- 14 H. Zhou, Q. Yao, S. Yuan, J. Liu and H. Deng, Phase relationships in the La–Ni–Si system at 673 K, *J. Alloys Compd.*, 2004, **366**(1), 161–164, DOI: [10.1016/S0925-8388\(03\)00698-4](#).
- 15 M. Pani, P. Manfrinetti, A. Provino, F. Yuan, Y. Mozharivskiy, A. V. Morozkin, A. V. Knotko, A. V. Garshev, V. O. Yapaskurt and O. Isnard, New tetragonal derivatives of cubic NaZn_{13} -type structure: RNi_6Si_6 compounds, crystal structure and magnetic ordering ($\text{R}=\text{Y}, \text{La}, \text{Ce}, \text{Sm}, \text{Gd}-\text{Yb}$), *J. Solid State Chem.*, 2014, **210**(1), 45–52, DOI: [10.1016/j.jssc.2013.10.046](#).
- 16 Y. M. Prots and W. Jeitschko, Lanthanum Nickel Silicides with the General Formula $\text{La}_{(n+1)(n+2)}\text{Ni}_{n(n-1)+2}\text{Si}_{n(n+1)}$ and Other Series of Hexagonal Structures with Metal:Metalloid Ratios Close to 2:1, *Inorg. Chem.*, 1998, **37**(21), 5431–5438, DOI: [10.1021/ic980397w](#).
- 17 H. Fujii, Structure and superconductivity of the ternary intermetallics of $\text{La}_3\text{Ni}_4\text{Si}_4$, $\text{La}_3\text{Ni}_4\text{Ge}_4$, and $\text{La}_3\text{Pd}_4\text{Si}_4$, *J. Phys.: Condens. Matter*, 2006, **18**(34), 8037–8047, DOI: [10.1088/0953-8984/18/34/015](#).
- 18 J. Liang and J. Zhao, The influence of Si on phase relation and hydrogen absorption properties of LaNi_5 , *Acta Phys. Sin.*, 1986, **35**, 505–511, DOI: [10.7498/aps.35.505](#).
- 19 F. Meli, A. Züttel and L. Schlapbach, Surface and bulk properties of $\text{LaNi}_{5-x}\text{Si}_x$ alloys from the viewpoint of battery applications, *J. Alloys Compd.*, 1992, **190**(1), 17–24, DOI: [10.1016/0925-8388\(92\)90167-8](#).
- 20 M. L. Fornasini and F. Merlo, The crystal structure of $\text{Ca}_2\text{Cu}_2\text{Ga}$, CaCuGa , SrCu_2Ga and BaCu_2Ga , *J. Less-Common Met.*, 1988, **142**, 289–294, DOI: [10.1016/0022-5088\(88\)90187-7](#).



- 21 E. Hovestreydt and E. Parthe, Hexapraseodymium heptanickel tetrasilicide, $\text{Pr}_6\text{Ni}_7\text{Si}_4$, an intergrowth of ThSi_2 - and $\text{Y}_3\text{Rh}_2\text{Si}_2$ -type slabs, *Acta Crystallogr., Sect. C: Cryst. Struct. Commun.*, 1984, **40**(12), 1992–1995, DOI: [10.1107/S0108270184010362](#).
- 22 L. Krause, R. Herbst-Irmer, G. M. Sheldrick and D. Stalke, Comparison of silver and molybdenum microfocus X-ray sources for single-crystal structure determination, *J. Appl. Crystallogr.*, 2015, **48**(1), 3–10, DOI: [10.1107/S1600576714022985](#).
- 23 G. Sheldrick, SHELXT - Integrated space-group and crystal-structure determination, *Acta Crystallogr., Sect. A: Found. Adv.*, 2015, **71**(1), 3–8, DOI: [10.1107/S2053273314026370](#).
- 24 G. Sheldrick, Crystal structure refinement with SHELXL, *Acta Crystallogr., Sect. C: Struct. Chem.*, 2015, **71**(1), 3–8, DOI: [10.1107/S2053229614024218](#).
- 25 L. Gelato and E. Parthé, STRUCTURE TIDY—a computer program to standardize crystal structure data, *J. Appl. Crystallogr.*, 1987, **20**(2), 139–143.
- 26 O. K. Andersen and O. Jepsen, Explicit, First-Principles Tight-Binding Theory, *Phys. Rev. Lett.*, 1984, **53**(27), 2571–2574.
- 27 R. Tank, O. Jepsen, A. Burkhardt and O. Andersen, *TB-LMTO-ASA Program*, Max-Planck-Institut für Festkörperforschung, Stuttgart, Germany, 1994.
- 28 M. Zwierzycki and O. Andersen, The overlapping muffin-tin approximation, *Acta Phys. Pol., A*, 2009, **115**, 64–68.
- 29 R. Dronskowski and P. E. Bloechl, Crystal orbital Hamilton populations(COHP): energy-resolved visualization of chemical bonding in solids based on density-functional calculations, *J. Phys. Chem.*, 1993, **97**(33), 8617–8624, DOI: [10.1021/j100135a014](#).
- 30 G. Kresse, M. Marsman and J. Furthmüller, *Vienna Ab Initio Simulation Package(VASP), The User Guide*, 2010.
- 31 V. Smetana, S. Steinberg, Y. Mudryk, V. Pecharsky, G. J. Miller and A.-V. Mudring, Cation-Poor Complex Metallic Alloys in $\text{Ba}(\text{Eu})\text{-Au-Al}(\text{Ga})$ Systems: Identifying the Keys that Control Structural Arrangements and Atom Distributions at the Atomic Level, *Inorg. Chem.*, 2015, **54**(21), 10296–10308, DOI: [10.1021/acs.inorgchem.5b01633](#).
- 32 E. T. Teatum, K. A. Gschneidner Jr and J. T. Waber, *Compilation of calculated data useful in predicting metallurgical behavior of elements in binary alloys systems Los Alamos Scientific Laboratory Report LA-4003, UC-25 Metals, Ceramics, and Materials TID-4500*, 1968.
- 33 J. Glaser, Neue Verbindungen im System Ca/Ni/Si , *Z. Anorg. Allg. Chem.*, 2002, **628**(9–10), 1946–1950, DOI: [10.1002/1521-3749\(200209\)628:9/10<1946::AID-ZAAC1946>3.0.CO;2-I](#).
- 34 K. A. Gschneidner Jr, in *Solid State Physics, Advances in Research and Applications*, ed. F. Seitz and D. Turnbull, New York, NY, 1957, ch. 4, pp. 275–426.
- 35 Y. M. Prots, J. Stępień-Damm, P. S. Salamakha and O. I. Bodak, The crystal structure of orthorhombic $\text{Ce}_3\text{Rh}_3\text{Si}_2$, an intergrowth of FeB - and Yp_2Si -type slabs, *J. Alloys Compd.*, 1997, **256**(1), 166–169, DOI: [10.1016/S0925-8388\(96\)02953-2](#).
- 36 V. Smetana, J. D. Corbett and G. J. Miller, Four polyanionic compounds in the K-Au-Ga system: a case study in exploratory synthesis and of the art of structural analysis, *Inorg. Chem.*, 2012, **51**(3), 1695–1702, DOI: [10.1021/ic201999u](#).
- 37 V. Smetana, G. J. Miller and J. D. Corbett, Three Alkali-Metal–Gold–Gallium Systems. Ternary Tunnel Structures and Some Problems with Poorly Ordered Cations, *Inorg. Chem.*, 2012, **51**(14), 7711–7721, DOI: [10.1021/ic300740u](#).
- 38 B. Li and J. D. Corbett, Different Cation Arrangements in Au-In Networks. Syntheses and Structures of Six Intermetallic Compounds in Alkali-Metal– Au-In Systems, *Inorg. Chem.*, 2007, **46**(15), 6022–6028, DOI: [10.1021/ic700519c](#).
- 39 W. Thronberens, H.-D. Sinnen and H.-U. Schuster, Ternäre Phasen der alkalimetalle mit palladium beziehungsweise platin und silizium, germanium beziehungsweise zinn mit kanal-strukturen, *J. Less-Common Met.*, 1980, **76**(1), 99–108, DOI: [10.1016/0022-5088\(80\)90013-2](#).
- 40 V. Smetana, M. Rhodehouse, G. Meyer and A.-V. Mudring, Gold polar intermetallics: structural versatility through exclusive bonding motifs, *Acc. Chem. Res.*, 2017, **50**(11), 2633–2641, DOI: [10.1021/acs.accounts.7b00316](#).
- 41 A. Brown, MX_2 compounds of thorium and the polymorphism of thorium disilicide, *Acta Crystallogr.*, 1961, **14**(8), 860–865, DOI: [10.1107/S0365110X61002497](#).
- 42 J. M. Moreau, D. Paccard and L. Paccard, Dirhodium triyttrium disilicide, $\text{Y}_3\text{Rh}_2\text{Si}_2$, *Acta Crystallogr., Sect. C: Cryst. Struct. Commun.*, 1984, **40**(8), 1311–1312, DOI: [10.1107/S0108270184007770](#).
- 43 W. A. Crichton, M. Mezouar, G. Monaco and S. Falconi, Phosphorus: New in situ powder data from large-volume apparatus, *Powder Diff.*, 2003, **18**(2), 155–158, DOI: [10.1154/1.1545115](#).
- 44 B. Cordero, V. Gomez, A. E. Platero-Prats, M. Reves, J. Echeverria, E. Cremades, F. Barragan and S. Alvarez, Covalent radii revisited, *Dalton Trans.*, 2008, 2832–2838, DOI: [10.1039/B801115J](#).
- 45 A. L. Allred, Electronegativity values from thermochemical data, *J. Inorg. Nucl. Chem.*, 1961, **17**(3), 215–221, DOI: [10.1016/0022-1902\(61\)80142-5](#).
- 46 V. Smetana, Q. Lin, D. K. Pratt, A. Kreyssig, M. Ramazanoglu, J. D. Corbett, A. I. Goldman and G. J. Miller, A Sodium-Containing Quasicrystal: Using Gold To Enhance Sodium's Covalency in Intermetallic Compounds, *Angew. Chem., Int. Ed.*, 2012, **51**(51), 12699–12702, DOI: [10.1002/anie.201207076](#).
- 47 I. Bigun, S. Steinberg, V. Smetana, Y. Mudryk, Y. Kalychak, L. Havela, V. Pecharsky and A.-V. Mudring, Magnetocaloric Behavior in Ternary Europium Indides EuT_5In : Probing the Design Capability of First-Principles-Based Methods on the Multifaceted Magnetic Materials, *Chem. Mater.*, 2017, **29**(6), 2599–2614, DOI: [10.1021/acs.chemmater.6b04782](#).
- 48 A. Provino, S. Steinberg, V. Smetana, U. Paramanik, P. Manfrinetti, S. K. Dhar and A.-V. Mudring, Gold in the layered structures of $\text{R}_3\text{Au}_7\text{Sn}_3$: from relativity to versatility, *Cryst. Growth Des.*, 2016, **16**(10), 5657–5668, DOI: [10.1021/acs.cgd.6b00478](#).



- 49 A. Ovchinnikov, V. Smetana and A.-V. Mudring, Metallic alloys at the edge of complexity: structural aspects, chemical bonding and physical properties, *J. Phys.: Condens. Matter*, 2020, **32**(24), 243002, DOI: [10.1088/1361-648x/ab6b87](https://doi.org/10.1088/1361-648x/ab6b87).
- 50 V. Smetana, J. D. Corbett and G. J. Miller, $\text{Na}_8\text{Au}_{9.8(4)}\text{Ga}_{7.2}$ and $\text{Na}_{17}\text{Au}_{5.87(2)}\text{Ga}_{46.63}$: The diversity of pseudo 5-fold symmetries in the Na–Au–Ga system, *J. Solid State Chem.*, 2013, **207**, 21–28, DOI: [10.1016/j.jssc.2013.08.017](https://doi.org/10.1016/j.jssc.2013.08.017).
- 51 U. Zachwieja, $\text{Na}_8\text{Au}_{11}\text{In}_6$: ein Gold - Indium-Polyedergerüst mit pentagonal-bipyramidalen AuAu_5In -Baueinheiten, *Z. Anorg. Allg. Chem.*, 1996, **622**(9), 1581–1586, DOI: [10.1002/zaac.19966220922](https://doi.org/10.1002/zaac.19966220922).
- 52 V. Smetana, G. J. Miller and J. D. Corbett, Polyclusters and Substitution Effects in the Na–Au–Ga System: Remarkable Sodium Bonding Characteristics in Polar Intermetallics, *Inorg. Chem.*, 2013, **52**(21), 12502–12510, DOI: [10.1021/ic401580y](https://doi.org/10.1021/ic401580y).

